STM Imaging of Impurity Resonances on Bi$_2$Se$_3$

Zhanybek Alpichshev,[1,2,3] Rudro R. Biswas,[4] Alexander V. Balatsky,[5,6] J. G. Analytis,[1,2] J.-H. Chu,[1,2]
I. R. Fisher,[1,2,7] and A. Kapitulnik[1,2,3,7]

[1]*Stanford Institute for Materials and Energy Sciences, SLAC National Accelerator Laboratory,*
2575 Sand Hill Road, Menlo Park, California 94025, USA
[2]*Geballe Laboratory for Advanced Materials, Stanford University, Stanford, California 94305, USA*
[3]*Department of Physics, Stanford University, Stanford, California 94305, USA*
[4]*Department of Physics, Harvard University, Cambridge Massachusetts 02138, USA*
[5]*Theoretical Division, Los Alamos National Laboratory, Los Alamos, New Mexico 87545, USA*
[6]*Center for Integrated Nanotechnologies, Los Alamos National Laboratory, Los Alamos, New Mexico 87545, USA*
[7]*Department of Applied Physics, Stanford University, Stanford, California 94305, USA*
(Received 29 July 2011; published 15 May 2012)

In this Letter we present detailed study of the density of states near defects in Bi$_2$Se$_3$. In particular, we present data on the commonly found triangular defects in this system. While we do not find any measurable quasiparticle scattering interference effects, we do find localized resonances, which can be well fitted by theory [R. R. Biswas and A. V. Balatsky, Phys. Rev. B **81**, 233405(R) (2010)] once the potential is taken to be extended to properly account for the observed defects. The data together with the fits confirm that while the local density of states around the Dirac point of the electronic spectrum at the surface is significantly disrupted near the impurity by the creation of low-energy resonance state, the Dirac point is not locally destroyed. We discuss our results in terms of the expected protected surface state of topological insulators.

Probing the interaction of quasiparticles with impurities and defects has proven to be a powerful tool for the study of electronic structure in solids. First, quasiparticle scattering from defects and impurities give rise to interference effects of electron waves associated with bands dispersion of the solid. In addition, impurities and defects can also result in bound states that induce localized resonances. For surface state bands (SSB), both phenomena are most suitably studied using scanning tunneling microscopy (STM) and spectroscopy (STS) [1–3]. In the case of topological insulators (TI) [4,5], probing quasiparticle scattering interference (QPI) and resonance scattering phenomena are expected to be particularly revealing, given that our focus is on the unusual properties expected from the SSB of these materials.

Much of the recent STM work on impurity and defect scattering in TI systems concentrated on Bi$_{1-x}$Sb$_x$ [6] and Bi$_2$Te$_3$ [7,8]. Indeed, within the main part of the SSB, exhibiting convex contour, oscillations were shown to be strongly damped, supporting the hypothesis of topological protection. However, oscillations do appear in the upper part of the SSB exhibiting concave contour [7], which disperse with a particular nesting wave vector corresponding to the allowed spin states of the warped contour [9]. In contrast, the cross-sectional contours of the SSB in Bi$_2$Se$_3$ are invariably convex, and together with weak scattering amplitude for non-time-reversed states could explain the lack of QPI, despite the observation of local impurities and defects in this system [10,11]. However, these defects do

affect the local surface potential and therefore should also affect the local density of states (LDOS), exhibiting resonance phenomena similar to d-wave superconductors [12] and graphene [13].

In this Letter we present a detailed study of defects-induced resonance states on the surface of the 3D topological insulator Bi$_2$Se$_3$ [14,15]. Different defects are studied, all showing evidence for the creation of low-energy resonance states which vary in strength but do not locally destroy the Dirac point. We further show that the main features of the data are captured by a simple extension of theoretical analysis of point-impurity scattering in the presence of Dirac dispersion [16], thus stressing the robustness of the SSB. In particular, we present high resolution topography and spectroscopy studies of resonance states associated with the frequently observed triangular defects, while also making a direct connection between their occurrence and the samples bulk doping.

Single crystals of Bi$_2$Se$_3$ were grown by slow cooling a binary melt as described elsewhere [17], yielding samples with typical dimensions of $2 \times 1 \times 0.1$ mm^3. The trigonal c axis is perpendicular to the cleavage plane of the crystals. Low magnetic field Hall measurements of similar undoped samples indicated n-type doping of $\sim 1 \times 10^{19}$ carriers/cm^3 which is a result of Se deficiency [17,18]. In this Letter we also show results on Sb-doped samples. These lower carrier density samples (about 100 times lower), with much reduced triangular defects, were obtained by slow cooling a ternary melt containing

progressively more Sb. Although Sb is isovalent with Bi, its substitution acts to control the defect density in the bulk crystals, reducing the bulk carrier density [19].

Samples were cleaved in vacuum of better than 5×10^{-10} torr, and quickly lowered to the ~ 8 K section of the microscope, where cryopumping ensures that the surface remains free from adsorbates for weeks or longer. Topography scans were taken at several bias voltages and set point currents (typically $+ 100$ mV and 60 pA). Tips used were made of PtIr. Figure 1 shows a 1600×1000 Å^2 topograph of the unoccupied states at the surface of cleaved undoped Bi$_2$Se$_3$ crystal. Similar to previous studies of undoped Bi$_2$Se$_3$ crystals [10,11], we observe a large concentration of triangular defects, uniquely oriented, with similar size but different brightness. High resolution topographs of the brightest triangular defects (see inset of Fig. 1) revealed a structure of six "bumps," each about ~ 0.1 Å high, separated by a distance of 8.2 ± 0.2 Å, corresponding to twice the hexagonal lattice constant of Bi$_2$Se$_3$. Less intense triangles have the same spatial structure but are weaker in strength. Assuming Se vacancies as the main source of defects in our samples [17], we can interpret the triangular structures as a response to the Se vacancies in different layers beneath the surface. As we will argue below, this interpretation is further supported by an earlier study of Urazhdin *et al.* [20], where excess Bi was introduced to Bi$_2$Se$_3$ crystals, producing clover-shaped defects in the occupied-states topographs, with the same dimensions as the triangular defects. Detailed calculations of these defects [20] suggested that they result from antisite doping where a Bi atom replaces a Se atom in the bottom Se layer of the top quintuple stack. The fact that resonance states can be identified in that paper [see Fig. 3(a) in [20]], with opposite charge compared to our data below, further supports our proposal. Counting ~ 60
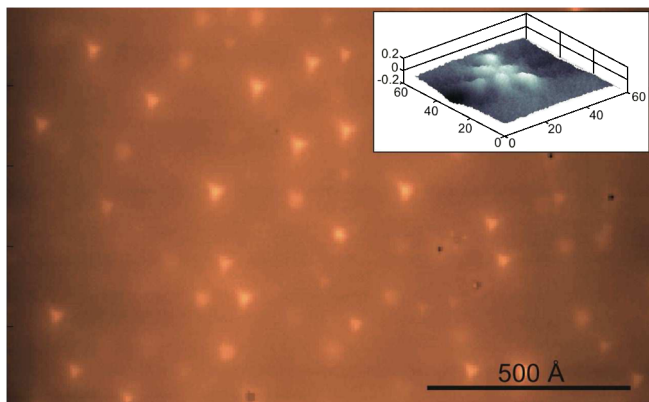
triangular defects in this topograph, and assuming that they all come from within the first quintuple layer, each donating two electrons per defect, we find a bulk carrier density of $\sim 6 \times 10^{18}$ carriers/cm^3 similar to the one deduced from Hall effect. The much reduced triangular defects found for the Sb-doped samples, for which also the bulk carrier density is low, supports this scenario.

Figure 2 depicts a topograph of a region containing several triangular defects, together with LDOS maps at three energies: within the bulk conduction band (BCB) [Fig. 2(b)], in the middle of the exposed Dirac-SSB [Fig. 2(c)], and below the Dirac point within the bulk valence band (BVB) [Fig. 2(d)]. In analyzing these maps (and many similar maps we studied), we concentrate on two triangular defects with different brightness, corresponding to a different apparent height. The first thing to notice is that while LDOS at energy values belonging the BCB is clearly enhanced on the defect site [Fig. 2(b)], the LDOS of the BVB is suppressed [Fig. 2(d)]. This indicates that the defect site is positively charged, which again is confirmed by the fact that our undoped Bi$_2$Se$_3$ is n type. However, the most interesting behavior is found within the exposed Dirac-SSB. As is seen in Fig. 2(c), three clear LDOS peaks around the triangular defects are formed, whose intensity strongly depend on energy. Although the lack of QPI implies a suppression of backscattering, the residual scattering of other momentum-transfer wave vectors adds up to give rise to a resonance state [16].

The Sb-doped Bi$_2$Se$_3$ samples show reduced density of triangular defects, but exhibit other types of defects. Figure 3 shows a topograph of a typical defect (presumably Sb cluster) and LDOS maps of the same region. Here again, for energies belonging to the BCB and BVB, the

FIG. 1 (color online). 1600×1000 Å^2 topograph of the surface of undoped Bi$_2$Se$_3$. Most impurities are triangular (typical one marked), pointing in the same direction, and are a consequence of subsurface Se vacancies [10,11]. The inset shows a three dimensional rendering of a triangular defect. The image was taken at bias voltage $V_b = +300$ mV and $I_s = 25$ pA.
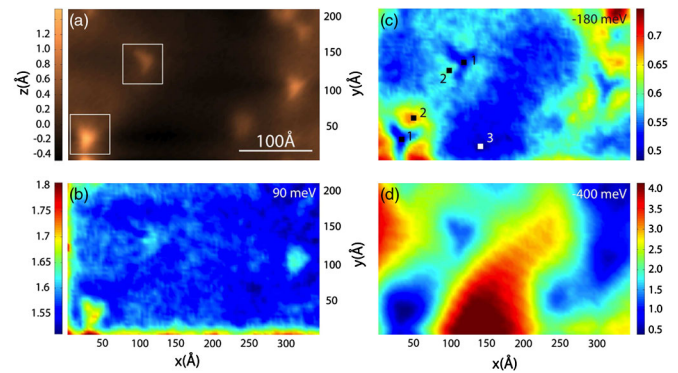
FIG. 2 (color online).   A topograph (a), and selected energy maps emphasizing two triangular impurities with different intensity, while both are the same size, bright triangle corresponds to a stronger protrusion than the faint one. LDOS at different energies are shown in panels (b), (c), and (d). [Points 1, 2, and 3 in (c) mark the center of defect, side resonance, and background, respectively.] Data were taken using $V_b = +100$ mV and $I_s = 80$ pA. Colored bars' scale is normalized by the LDOS at zero bias at the location of point 3.
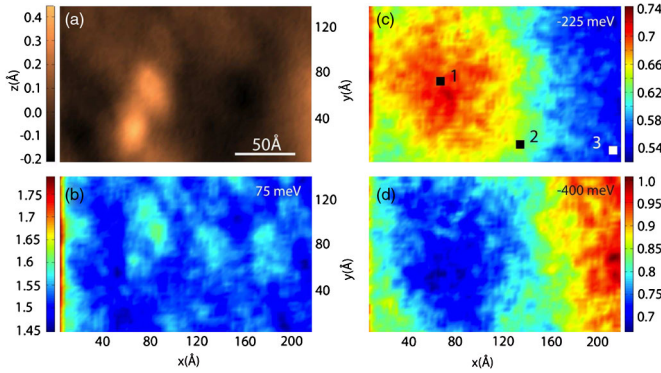
FIG. 3 (color online). A topograph (a), and selected energy maps emphasizing an extended impurity in Sb-doped Bi_2Se_3. LDOS at different energies are shown in panels (b), (c), and (d). (Points 1, 2, and 3 mark the center of the defect, the edge of its extent, and background, respectively.) Data were taken using $V_b = 400$ mV and $I_s = 70$ pA. Colored bars' scale is normalized by the LDOS at zero bias at the location of point 3.

LDOS in the vicinity of the defect is depressed, while a strong LDOS peak, now spread around the impurity site, appears in the bulk gap [Fig. 3(c)].

Figure 4(a) shows tunneling spectroscopies on the triangular impurity sites ("bright" and "faint"), with a spectrum away from defects shown for reference [21]. Figure 4(b) shows the difference between those curves, showing a broad resonance peak that is located at positive bias as compared to the Dirac point. Both resonances are rather similar in shape, and we emphasize here that similar shape and width have been measured for many triangular defects with a variety of "brightness" on several different samples. Figure 4(c) shows LDOS on top of the defect
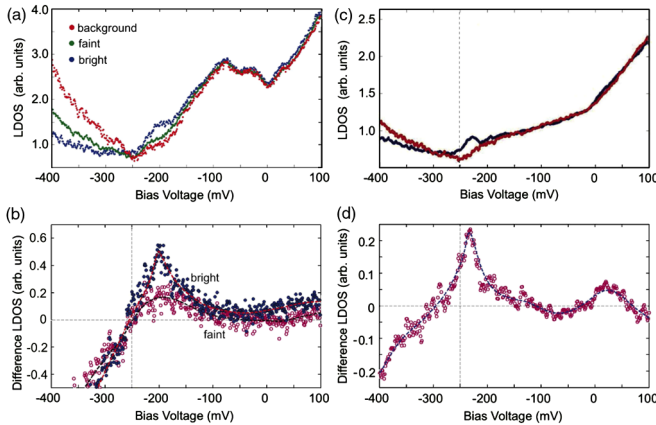

FIG. 4 (color online). Emergence of a resonance near the Dirac point for two different impurities; (a) triangular defects corresponding to the bright and faint of Fig. 2, with the difference LDOS for both defects shown in (b); (c) extended defect in Sb-doped Bi_2Se_3 (Fig. 3), and the difference LDOS shown in (d). Dashed lines mark the location of the Dirac point which is identified as the position of DOS minimum.

shown in Fig. 3 on a Sb-doped crystal, together with the LDOS away from the impurity. Figure 4(d) shows the difference curve for these two spectra, resulting in a much sharper and more pronounced resonance.

The general problem of impurity-potential scattering on the surface of a TI has been recently studied by Biswas and Balatsky [16]. Considering a two-dimensional Dirac gas interacting with a δ-function potential, they found that a resonance state is formed around any localized defect; the Dirac point is not destroyed by the scattering; and LDOS around the impurity falls of as $1/r^2$. Furthermore, the shape of the resonance is not Lorentzian and its width is determined by the strength of the potential which also sets the position of the resonance on the energy axis. As the strength of the potential is increased the peak gets narrower and moves towards the Dirac point. While neither the triangular defects nor the Sb cluster, can be approximated by a δ-function potential, we assume that the net effect on the SSB may still be similar, especially if we look at the LDOS slightly away from the center of the defect. However, to account for the extended nature of the defect we modify the calculations of Ref. [16], with a step potential replacing the local δ-function potential. The step potential is parametrized with a height $V = V_0$, extending over a radius R_0, and zero everywhere else. Using a step potential, the strength of the impurity is therefore characterized by the product $V_0 R_0^2$, rather than the potential height itself. The extent of the potential (R_0) is further checked against the topography and the LDOS in the exposed part of the Dirac band. In particular, since the center of the triangular impurity shows suppressed LDOS, the "on-site" LDOS for these impurities are calculated as an average between the LDOS at the center and the LDOS at the three peaks surrounding it [shown in Fig. 5(a)]. Figures 5(b) and 5(c) show typical fits to the measured LDOS difference for both triangular and Sb-cluster defects.

The first thing that we notice is that the quality of the fit is visibly better for a triangular defect [Fig. 5(b)] compared to the extended defect on the surface of an Sb-doped sample [Fig. 5(d)]. We believe that this is due to the fact that the triangular defects are more compact in space and are therefore better described as a local perturbation. The Sb cluster, on the other hand, is a significantly extended object whose effect might not be described as a simple potential interaction with SSB. For example, in a recent study of an extended step on the surface of Bi_2Te_3 we have shown that a "bound state" is formed as a consequence of interference in the bulk due to the finite penetration depth of the SSB [22]. Specifically, an important feature of the theory is the protection of the Dirac point against the perturbation due to the impurity. Here, assuming that the background incoherent LDOS is uniform in space and only weakly energy dependent, the difference between the LDOS affected by the defect and
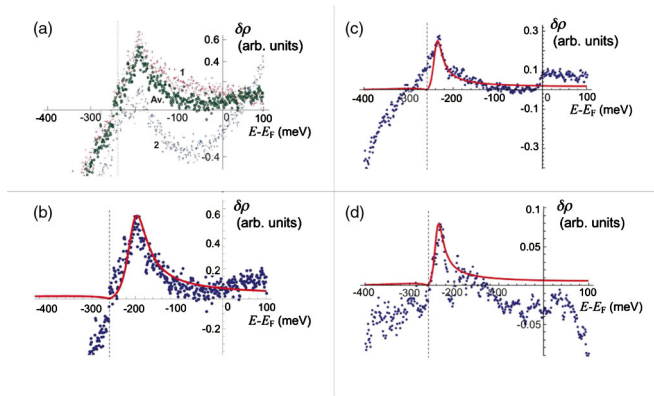
FIG. 5 (color online).   Theoretical fits to resonance amplitudes.
(a) Raw LDOS difference data for a bright triangle where
(1) represents the middle of the triangle and (2) represents the
side peaks [see Fig. 2(c)]. The averaged data are marked with
Av; (b) averaged data from (a), fitted to theory (see text)
with $V_0 = 3.17$ eV, $R = 15$ Å; (c) fit to extended defect on an
Sb-doped sample, at center of defect [point (1) in Fig. 3] with
$V_0 = 0.71$ eV, $R = 64$ Å; (d) same parameters as for (c), but
away from center of defect [point (2) in Fig. 3] (see text). Dashed
lines mark the location of the Dirac point.

the bare LDOS (far away from any defects) should be
equal to zero at the Dirac point energy. While this prop-
erty is observed on triangular impurities, the Sb-cluster
impurity shows excess scattering near the Dirac point,
shifting the zero of the difference-LDOS ($\delta\rho$) by about
30 meV. However, as is seen in Fig. 5(d) away from the
center of the defect the fit becomes much better, including
the location of the Dirac point (zero crossing). It also
illustrates the qualitative fact that this resonance being
situated closer to the Dirac point compared to the one on
Fig. 5(b) is also narrower than the latter signaling we are
having a stronger scatterer.

Focusing on the triangular impurities, we already men-
tioned that they appear with a variety of strengths related to
their different protrusion heights (see Fig. 1). A surprising
result, which is revealed when we examine the LDOS
difference of the bright and faint triangular defects, is
that they have the same scattering strength as both posi-
tions of the associated resonances and their peaks widths
are the same within the error bars. This is in a good
agreement with the suggestion that all triangle impurities
have similar origin.

Finally, we show in Fig. 6 the dependence of the LDOS
at the energy of the resonance of the broad scatterer
(Sb cluster) on the distance away from the impurity center.
Fitting the decay as a function of distance, we find it hard to
determine the exact power law decay. In Fig. 6 we show an
averaged decay for the Sb-cluster defect, fitted with both
$1/r$ and $1/r^2$. While the $1/r$ decay fits the data better all the
way to the extent of the defect, the two power laws, and in
fact any power law in between, may still be a good
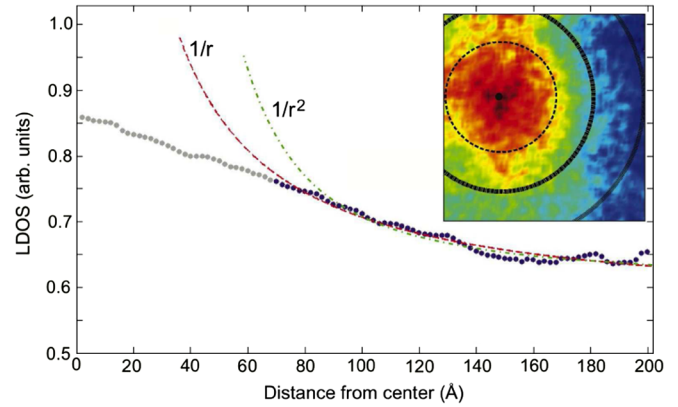description of the data, especially considering the large

FIG. 6 (color online).   LDOS as a function of distance from the
center of the impurity. The dashed line is a fit to $1/r$ for the dark
points (after ~ 65 Å) and the dash-dotted line is a fit to $1/r^2$.
The inset shows the contours of decay of the LDOS around the
impurity center (●) at 65, 100, and 150 Å.

characteristic length for Bi_2Se_3 surface state ($\lambda \sim 30$ Å
[8]). In particular the data rules out an exponential decay
of the LDOS resonance with λ, which is another confirma-
tion of the two-dimensional nature of the band giving rise
to the resonance state.

In conclusion, we identified the resonance states asso-
ciated with the triangular impurities in Bi_2Se_3. We found
that independent of their observed intensity, these impuri-
ties induce resonances of similar shape and strength, and
thus can be considered as a characteristic of Bi_2Se_3 (and
possibly also other members of this family such as Bi_2Te_3)
spectroscopy. We further showed that other type of defects,
extended in nature, also give rise to resonant states.
Comparing the various defect resonances to each other
and with theory, we conclude that a simple scattering
mechanism in the presence of a Dirac-type 2D quasipar-
ticles gives a full account to the observed data. While
theoretical curves fitted the data very well for the case of
the triangular defects, we find that for stronger, more
extended defects, some modifications are needed that
may include the finite penetration depth of the surface
state.

[1] M. F. Crommie, C. P. Lutz, and D. M. Eigler, Nature
(London) **363**, 524 (1993).
[2] Y. Hasegawa and Ph. Avouris, Phys. Rev. Lett. **71**, 1071
(1993).

P H Y S I C A L   R E V I E W   L E T T E R S

[3] P. T. Sprunger, L. Petersen, E. W. Plummer, E. Lægsgaard, and F. Besenbacher, Science **275**, 1764 (1997).

[4] Xiaoliang Qi and Shoucheng Zhang, Phys. Today **63**, No. 1, 33 (2010); Rev. Mod. Phys. **83**, 1057 (2011).

[5] M. Z. Hasan and C. L. Kane, Rev. Mod. Phys. **82**, 3045 (2010).

[6] P. Roushan, J. Seo, C. V. Parker, Y. S. Hor, D. Hsieh, D. Qian, A. Richardella, M. Z. Hasan, R. J. Cava, and A. Yazdani, Nature (London) **460**, 1106 (2009).

[7] Z. Alpichshev, J. G. Analytis, J.-H. Chu, I. R. Fisher, Y. L. Chen, Z. X. Shen, A. Fang, and A. Kapitulnik, Phys. Rev. Lett. **104**, 016401 (2010).

[8] T. Zhang, P. Cheng, Xi Chen, J.-F. Jia, X. Ma, K. He, L. Wang, H. Zhang, Xi Dai, Z. Fang, X.-C Xie, and Qi-Kun Xue, Phys. Rev. Lett. **103**, 266803 (2009).

[9] Liang Fu, Phys. Rev. Lett. **103**, 266801 (2009).

[10] S. Urazhdin, D. Bilc, S. D. Mahanti, S. H. Tessmer, Theodora Kyratsi, and M. G. Kanatzidis, Phys. Rev. B **69**, 085313 (2004).

[11] Y. S. Hor, A. Richardella, P. Roushan, Y. Xia, J. G. Checkelsky, A. Yazdani, M. Z. Hasan, N. P. Ong, and R. J. Cava, Phys. Rev. B **79**, 195208 (2009).

[12] A. V. Balatsky, I. Vekter, and J. X. Zhu, Rev. Mod. Phys. **78**, 373 (2006).

[13] M. M. Ugeda, I. Brihuega, F. Guinea, and J. M. Gomez-Rodriguez, Phys. Rev. Lett. **104**, 096804 (2010).

[14] H. Zhang, C.-X. Liu, X.-L. Qi, X. Dai, Z. Fang, and S.-C. Zhang, Nature Phys. **5**, 438 (2009).

[15] D. Hsieh, Y. Xia, D. Qian, L. Wray, J. H. Dil, F. Meier, J. Osterwalder, L. Patthey, J. G. Checkelsky, N. P. Ong, A. V. Fedorov, H. Lin, A. Bansil, D. Grauer, Y. S. Hor, R. J. Cava, and M. Z. Hasan, Nature (London) **460**, 1101 (2009).

[16] Rudro R. Biswas and Alexander V. Balatsky, Phys. Rev. B **81**, 233405(R) (2010).

[17] J. G. Analytis, J-H. Chu, Y. Chen, F. Corredor, R. D. McDonald, Z. X. Shen, and I. R. Fisher, Rev. Bras. Fis. **81**, 205407 (2010).

[18] J. Horák, Z. Starý, P. Lošťák, and J. Panciř, J. Phys. Chem. Solids **51**, 1353 (1990).

[19] P. Lošťák, Č. Drašar, H. Süssmann, P. Reinshaus, R. Novotný, and L. Beneš, J. Cryst. Growth **179**, 144 (1997).

[20] S. Urazhdin, D. Bilc, S. H. Tessmer, S. D. Mahanti, Theodora Kyratsi, and M. G. Kanatzidis, Phys. Rev. B **66**, 161306(R) (2002).

[21] Note that for Bi_2Se_3 the Dirac point is exposed, and thus one would expect energy-linear LDOS that vanish at the Dirac point. However, a large background LDOS, presumably incoherent in nature, shifts the Dirac point to a large LDOS value, a fact that needs to be taken into account when any data involving the SSB is analyzed.

[22] Z. Alpichshev, J. G. Analytis, J.-H. Chu, I. R. Fisher, and A. Kapitulnik, Phys. Rev. B **84**, 041104 (2011).